Comparing Landsat-7 ETM+ and ASTER Imageries to Estimate Daily Evapotranspiration Within a Mediterranean Vineyard Watershed

Carlo Montes, Frédéric Jacob

HAL Id: hal-03736788
https://hal.science/hal-03736788

Submitted on 22 Jul 2022

Comparing Landsat-7 ETM+ and ASTER Imageries to Estimate Daily Evapotranspiration Within a Mediterranean Vineyard Watershed

Carlo Montes and Frédéric Jacob, *Senior Member, IEEE*

Abstract—**We compared the capabilities of Landsat-7 Enhanced Thematic Mapper Plus (ETM+) and Advanced Spaceborne Thermal Emission and Reflection Radiometer (ASTER) imageries for mapping daily evapotranspiration (ET) within a Mediterranean vineyard watershed. We used Landsat and ASTER data simultaneously collected on four dates in 2007 and 2008, along with the Simplified Surface Energy Balance Index (S-SEBI) model. We used previously ground-validated good quality ASTER estimates as reference, and we analyzed the differences with Landsat retrievals in the light of instrumental factors and methodology. Although Landsat and ASTER retrievals of S-SEBI inputs were different, estimates of daily ET from the two imageries were similar. This is ascribed to the S-SEBI spatial differencing in temperature, and opens the path for using historical Landsat time series over vineyards.**

Index Terms—**Vineyard landscape, daily ET, solar and thermal infrared remote sensing, Landsat-7 ETM+, ASTER, S-SEBI.**

I. INTRODUCTION

ACCURATE estimation of daily actual evapotranspiration (ET) is essential for vineyards because grape yield and quality depend upon root zone moisture throughout the growth cycle. Solar and thermal infrared (TIR) remote sensing is valuable for characterizing daily ET in a spatially distributed manner. Besides, time series from long-term satellite missions permit to study the impacts of climate and land use changes, and to calibrate process models for long-term forecasting [1].

ET monitoring in vineyard landscapes requires a good characterization of land surface drivers in space and time [2-4]. This can be achieved with hourly frequency using geostationary sensors (e.g., Meteosat Second Generation / Spinning Enhanced Visible and Infrared Imager) or daily frequency using sun-synchronous sensors (e.g., Terra / Moderate Resolution Imaging Spectroradiometer), but the TIR data spatial resolutions limit applications to kilometric spatial scales [5]. When addressing field scale patterns, it is necessary to use sub-hectometric data [6]. This can be achieved disaggregating low-resolution imagery, but the loss of information associated

with fine-scale variabilities can lead to significant errors [7].

Advanced Spaceborne Thermal Emission and Reflection Radiometer (ASTER) and Landsat-7 Enhanced Thematic Mapper Plus (ETM+, referred to as Landsat hereafter) collect spaceborne TIR data with 90 m and 60 m spatial resolution, respectively. They permit to study field scale ET patterns, although the bi-weekly revisit induces the necessity to perform temporal interpolations for daily basis estimation [8].

ASTER punctually collects multispectral TIR data with high radiometric quality that permit to accurately estimate ET or its drivers [9, 10], also over vineyards [2, 3]. Landsat routinely collects single spectral band TIR data with moderate radiometric quality. Difficulties induced by low quality of TIR data can be overcome using spatial differencing in temperature [11]. Good results were obtained with Landsat over homogeneous canopies [e.g., 12, 13], but it is necessary to deepen recent works on row-structured vineyards [e.g., 4] for which shadow and multiple scattering can combine with data radiometric and spectral quality.

To evaluate the potential of Landsat data in estimating daily ET over vineyards, this letter aims to compare Landsat retrievals against previously ground-validated ASTER estimates. Daily ET is derived from both imageries using the Simplified Surface Energy Balance Index (S-SEBI) method that relies on spatial differencing in temperature [14], which can mitigate low radiometric quality of the Landsat TIR data. We present the study site and the data to be used, we explain the remote sensing procedures, and we finally compare the Landsat and ASTER retrievals for S-SEBI inputs and outputs.

II. STUDY AREA, DATA COLLECTION AND PREPROCESSING

A. Study Site

The study took place within the Peyne watershed in Languedoc-Roussillon, Southern France (43.49 N, 3.37 E, 80 m asl). The watershed is 65 km^2 size and mainly includes trellis-trained vineyards (70% of total area) under rainfed conditions (>95%), and in lesser extent annual crops, forests, shrubs and urban zones. Climate is Mediterranean with average rainfall of 650 mm y^{-1} and reference ET of 1105 mm y^{-1}.

Soils are highly heterogeneous in texture, depth and parent material, inducing significant differences in soil moisture regime and rooting depth. Watertable conditions within the rooting zone are contrasted, including absent, transient or permanent watertables during the growth cycle, which affects vineyard water status and resulting stress [15].

Carlo Montes is with IRD / UMR LISAH, Montpellier, France, and with NASA / GISS, New York City, NY, USA (e-mail: ccmontesv@gmail.com).

Frédéric Jacob is with IRD / UMR LISAH, Montpellier, France (e-mail: frederic.jacob@ird.fr).

B. In Situ Meteorological Data

A CIMEL ENERCO 400 weather station was set upon a 0.15 km^2-size vineyard plot within the Peyne watershed. It collected hourly meteorological data of air temperature, relative humidity, solar irradiance, wind speed and rainfall. On the same plot, a Campbell NT LITE device measured hourly net radiation. Devices were set up 2 m height above the ground.

C. ASTER official Products

We used ASTER official products [16] that included top of atmosphere (TOA) radiances over all spectral bands and Top of Canopy (TOC) biophysical variables: narrowband reflectance (15 and 30 m spatial resolution), narrowband emissivity and radiometric temperature (90 m spatial resolution). They corresponded to cloud-free images acquired at 10:30 local solar time in 2007 (10 May, 15 September) and 2008 (15 July, 01 September). These products are routinely generated by (1) conducting instrumental corrections, (2) atmospherically correcting TOA radiances over the solar and TIR spectral domains [17], and (3) applying the Temperature and Emissivity Separation algorithm on the TIR data [18].

D. Landsat-7 ETM+ official Products

Contrary to ASTER, raw data only are available for Landsat. We used four cloud-free Landsat imageries collected at 10:20 local solar time on the same dates as ASTER data. They include TOA radiance at 30 m (respectively 60 m) spatial resolution over the solar (respectively TIR) spectral domain. The study area was outside the imagery gaps induced by the SLC failure. We applied instrumental corrections using the calibration factors provided as metadata.

E. Atmospheric corrections of Landsat data

We used the Second Simulation of the Satellite Signal in the Solar Spectrum (6S) atmospheric radiative transfer model [19] to retrieve TOC narrowband reflectance over the solar domain. Following [20], we used the Moderate Resolution Atmospheric Radiance and Transmittance Model (MODTRAN) atmospheric radiative transfer code to derive TOC radiance from TOA radiance, where radiances over the TIR domain are expressed as brightness temperatures.

Both 6S and MODTRAN required information about the atmospheric state during the satellite overpass. We used atmospheric profiles on pressure, temperature and relative humidity from the National Centers for Environmental Prediction (NCEP) reanalysis [21], linearly interpolated to the center of the study site from the surrounding grid points. We estimated aerosol optical thickness (AOT) at 550 nm by linearly interpolating data at 440 nm and 675 nm from the Avignon site (43.932 N, 4.878 E, 32 m asl) of the AERONET network [22]. We extracted seasonal values for ozone and carbon dioxide concentrations from the 6S and MODTRAN databases.

III. RETRIEVAL OF DAILY ET FROM ASTER AND LANDSAT

We used S-SEBI to estimate daily ET from ASTER and Landsat imageries. Among existing methods based on spatial differencing in temperature [23], we choose this one because numerous studies previously showed it was feasible and robust when applied over areas that depict contrasts in water status.

A. Calculation of ASTER and Landsat S-SEBI Inputs

Input variables for S-SEBI were broadband albedo α over 0.3-3 μm, radiometric temperature T_S and net radiation R_n.

We derived S-SEBI inputs from ASTER products following [2]. We calculated α as a linear combination of TOC narrowband reflectances. Due to deficient shortwave infrared bands, we used the generic formulation proposed by [24], linearly corrected against that proposed by [25]. T_S corresponded to the ASTER official product. We calculated R_n from α, solar and atmospheric broadband irradiances, broadband emissivity ε_B, and T_S. We derived solar irradiance from meteorological measurements. We retrieved atmospheric broadband irradiance from meteorological measurements of air temperature and vapor pressure, following [26]. We estimated ε_B as a linear combination of narrowband emissivities, following [27].

We derived inputs variables from Landsat atmospherically corrected data. We calculated α as a linear combination of TOC narrowband reflectances by following [25]. We derived T_S from TOC brightness temperature, narrowband emissivity ε_N and atmospheric narrowband irradiance over band 6. We derived ε_N using the formulations proposed by [28-30]. We retrieved atmospheric narrowband irradiance from meteorological measurements of air temperature and vapor pressure, using the formulation proposed by [31]. We calculated R_n using the procedure implemented for ASTER imagery. For this, we assumed ε_B equaled ε_N by following [32].

B. Implementation of S-SEBI over Landsat and ASTER data

S-SEBI assumes that the study area depicts contrasted water statuses inducing a significant scattering in the T_S-α space [14]. For any pixel with T_S, evaporative fraction EF is estimated as $EF = (T_H - T_S) / (T_H - T_{ET})$. T_H (T_{ET}) is maximum (minimum) temperature within the same albedo class, corresponding to dry (wet) areas with very low (large) latent heat flux. Assuming instantaneous and daily EF are equal, and neglecting daily soil heat flux, daily ET is estimated as $ET = EF (R_{n,d} / \lambda)$. λ is latent heat of vaporization. $R_{n,d}$ is daily net radiation obtained from (1) in-situ data of R_n diurnal course and (2) Landsat / ASTER instantaneous retrievals of R_n [33].

We implemented S-SEBI over both imageries following [2, 3]. Within the T_S-α space, we estimated the dry (wet) limit corresponding to upper (lower) bound through a linear regression between albedo class value and T_H (T_{ET}). To avoid the exclusion of extreme pairs, we added (subtracted) an offset to dry (wet) limits, this offset being calculated as the standard deviation of T_H (T_{ET}) over all albedo classes.

Previous studies validated ASTER / S-SEBI retrievals of daily ET against ground-based data [2, 3]. The validation was conducted within the same study area, over a panel of seven locations that depicted a large range of vine water status. The observed differences between ground truth and ASTER / S-SEBI retrievals were 0.8 mm d^{-1} (30% relative).

TABLE I. STATISTICAL INDICATORS OBTAINED WHEN COMPARING LANDSAT AND ASTER RETRIEVALS. INDICATORS ARE BIAS AND RMSE, BOTH ABSOLUTE (IN QUANTITY UNITS) AND RELATIVE (%). COMPARISONS OF TOA RADIANCE ESTIMATES ARE GIVEN FOR MATCHING BANDS OVER THE SOLAR (COLUMN 3 TO 5, IN W M^{-2} SR^{-1} µM^{-1}) AND THE TIR (COLUMN 9, IN K FOR TOA BRIGHTNESS TEMPERATURE) DOMAINS. COMPARISONS OF RETRIEVALS OF NARROWBAND REFLECTANCE (NR) AND TOC BRIGHTNESS TEMPERATURE (BT) ARE GIVEN FOR MATCHING BANDS OVER THE SOLAR (COLUMN 6 TO 8) AND THE TIR (COLUMN 10, IN K) DOMAINS. AI STANDS FOR ASTER / BAND I, LJ STANDS FOR LANDSAT / BAND J. S-SEBI INPUTS ARE ALBEDO (α), RADIOMETRIC TEMPERATURE (T_S IN K), AND NET RADIATION (RN IN W M^{-2}). S-SEBI OUTPUTS ARE EVAPORATIVE FRACTION (EF) AND DAILY EVAPOTRANSPIRATION (ET IN MM D^{-1}).

	Date	TOA L2-A1	TOA L3-A2	TOA L4-A3	NR L2-A1	NR L3-A2	NR L4-A3	TOA BT L6-A14	TOC BT L6-A14	α	T_S	R_n	EF	ET
RMSE	10 May 2007	9.81	10.76	9.59	0.05	0.03	0.02	1.5	1.1	0.02	1.9	75	0.08	0.43
	15 Sep 2007	6.49	6.54	4.55	0.04	0.03	0.04	2.1	1.8	0.03	1.2	82	0.09	0.35
	15 Jul 2008	9.11	9.20	10.12	0.04	0.03	0.03	1.7	1.3	0.02	1.4	75	0.07	0.65
	01 Sep 2008	9.90	9.69	9.32	0.05	0.03	0.04	1.3	1.5	0.02	1.4	70	0.11	0.37
RRMSE	10 May 2007	15	19	12	31	20	7	-	-	10	-	14	15	15
	15 Sep 2007	13	15	8	29	21	11	-	-	13	-	15	19	24
	15 Jul 2008	15	18	12	30	21	8	-	-	11	-	14	13	21
	01 Sep 2008	19	21	14	38	21	13	-	-	10	-	14	21	19
Bias	10 May 2007	-7.27	-6.27	-8.23	-0.04	0.01	0.01	-1.1	-0.5	0.01	1.5	-72	0.05	-0.10
	15 Sep 2007	-4.96	-3.57	-2.76	-0.04	0.02	0.03	-2.0	-1.5	0.02	0.0	-79	0.02	-0.13
	15 Jul 2008	-7.10	-5.67	-8.48	-0.04	0.01	0.01	-1.4	-0.7	0.01	0.6	-70	0.01	-0.12
	01 Sep 2008	-8.41	-7.10	-8.11	-0.05	0.00	0.01	-1.0	-0.5	0.00	0.8	-57	0.07	0.03
RBias	10 May 2007	-11	-11	-10	-29	5	3	-	-	4	-	-14	9	-4
	15 Sep 2007	-10	-8	-5	-26	12	9	-	-	9	-	-15	4	-9
	15 Jul 2008	-12	-11	-10	-25	9	2	-	-	4	-	-13	2	-14
	01 Sep 2008	-16	-15	-12	-34	4	3	-	-	2	-	-13	14	2

IV. COMPARING LANDSAT AND ASTER IMAGERIES

A. Superimposing Landsat and ASTER Imageries

ASTER and Landsat spectral bands have different spatial resolutions. To compare their retrievals, we bi-linearly interpolated the imageries to 90 m. We next superimposed both imageries to a 0.5 m spatial resolution aerial orthophotograph collected in summer 2007, by using reference control points with the corresponding projection system (i.e., UTM).

B. Comparing Landsat and ASTER retrievals

We compared Landsat and ASTER retrievals for S-SEBI inputs and outputs. This aimed to link the differences on inputs and outputs, in relation to the S-SEBI spatial differencing in temperature. We also attempted to quantify error sources by comparing Landsat and ASTER products of TOA radiance, TOC narrowband reflectance and brightness temperature.

Previous validation exercises showed the good quality of the ASTER retrievals [2, 3]. Therefore, we conducted the intercomparison by considering the ASTER retrievals as the reference values and the Landsat retrievals as those to be evaluated. We conducted the comparison using bias and root mean square error (RMSE). Apart from temperature, we also calculated relative bias (RBias) / RMSE (RRMSE), as the ratio of bias / RMSE to the mean value of the ASTER estimate.

V. RESULTS AND DISCUSSION

A. Comparing Landsat and ASTER basic products

We first compared Landsat and ASTER estimates of TOA radiances, TOC narrowband reflectance and brightness temperature, for the spectral bands that roughly matched (Landsat bands 2, 3, 4, 6 versus ASTER bands 1, 2, 3, 14, respectively). We obtained very similar results when considering (1) ASTER band 14 only or (2) averaged values over ASTER bands 13 and 14. The results are displayed in Table I. In all cases, the unsystematic (or random) differences were low.

For TOA radiance over the solar domain, Landsat estimates were lower than ASTER ones, by 10% relative, and the biases were stable over time. For TIR TOA radiance (expressed as brightness temperature), Landsat estimates were lower than ASTER ones, and the biases changed over time by a factor of two. The differences between Landsat and ASTER estimates were ascribed to differences in sensor filters and calibrations.

For TOC narrowband reflectance, Landsat estimates differed from ASTER ones. Landsat estimates over band 2 (respectively 3 and 4) were lower (respectively larger) than ASTER estimates over band 1 (respectively 2 and 3). For a given set of ASTER / Landsat bands to be compared, the biases changed from one day to another, by 0% to 200% relative. For TOC brightness temperature, Landsat estimates were lower than ASTER ones, and the biases changed over time by a factor of three. The differences between ASTER and Landsat estimates were ascribed to differences in both TOA radiances and atmospheric corrections. Over the TIR domain, the differences in atmospheric corrections were ascribed to differences in atmospheric humidity profiles. Over the solar domain, the differences in atmospheric corrections were ascribed to differences in AOT at 550 nm and ozone concentration.

B. Comparing Landsat and ASTER S-SEBI Inputs

Table I also displays the comparison of Landsat and ASTER retrievals for S-SEBI inputs:

For α, the Landsat retrievals overestimated the ASTER ones. The bias magnitude was similar to those observed for TOC narrowband reflectances at 650 and 800 nm, which was ascribed to the weighting coefficients used for albedo calculation. Given the accuracy of the ASTER retrievals of R_n [2, 3], we were confident in the ASTER retrievals of α that drove 80% of R_n, and the overestimation of ASTER albedo by Landsat one was consistent with a recent validation exercise [34]. Overall, RRMSE values were comparable with previous validation exercises of albedo retrievals [35-37].

For T_S, the Landsat retrievals tended to overestimate the ASTER ones (Table I and Fig. 1a). The biases were different from those observed for TOC brightness temperature, which

was ascribed to emissivity calculation for row canopies. Over-all, the differences were similar to those reported by several validation and intercomparison studies [34, 38-40].

For R_n, the Landsat retrievals underestimated the ASTER ones. Larger differences between R_n retrievals corresponded to larger differences in α retrievals, which resulted from the influence of α on shortwave net radiation, the latter amounting to 80% of R_n. Overall, RRMSE values were similar to previous comparisons of R_n retrievals [9, 11, 34].

For the S-SEBI inputs, the RMSE and bias values were correlated. Similarly, we observed low scatterings within scatterplots for these inputs. Therefore, differences between Landsat and ASTER retrievals were systematic in a large extent.

Fig. 1. Comparison of Landsat and ASTER retrievals on 10 May 2007 for (a) radiometric temperature T_S and (b) daily ET. Scatterplots of (c) ASTER and (d) Landsat retrievals within the T_S - α space, to be used by S-SEBI when computing evaporative fraction EF. Continuous line in and is the 1:1 relationship and dashed line is the linear fit. Scatterplots are displayed as probability density function.
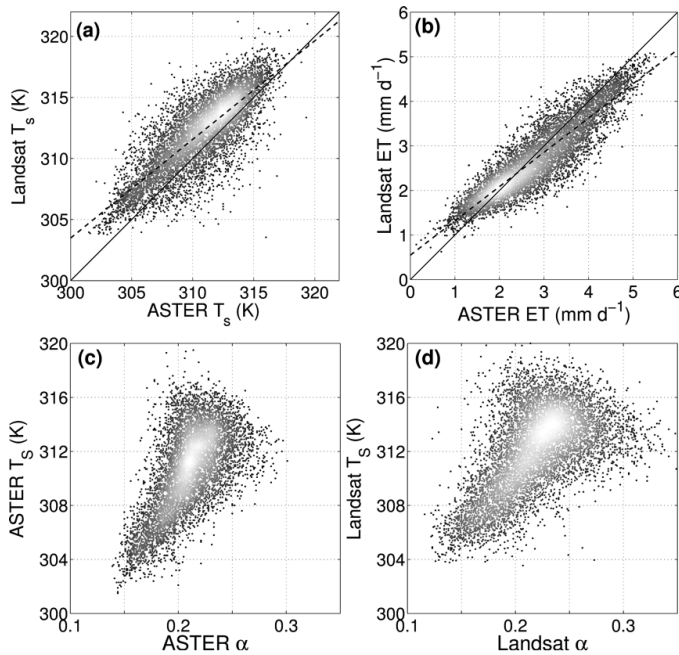
C. Comparing Landsat and ASTER S-SEBI outputs

Table I also displays differences between Landsat and ASTER retrievals of evaporative fraction (EF) and daily ET. We analyzed these differences in the light of those observed for S-SEBI inputs (α, T_S and R_n).

For EF, the Landsat retrievals overestimated the ASTER ones. We could not link the differences on EF retrievals with those observed on the S-SEBI inputs used to compute EF (α, T_S). This was ascribed to the spatial differencing in temperature on which relies S-SEBI, since it tended to offset differences in temperature. As compared to S-SEBI inputs, RMSE and bias values on EF were close and slightly correlated on a daily basis, while scatterplots depicted low scatterings. Thus, differences between Landsat and ASTER retrievals of EF were systematic in a moderate extent.

For daily ET, the Landsat retrievals tended to underestimate the ASTER ones. The differences between ET retrievals were quite correlated to those between R_n retrievals, but not to those between EF estimates. This was consistent with a previous study that reported small EF changes and large ET changes for a 35 % albedo change [41].

The average difference between daily ET retrievals from both imageries was about 0.45 mm d^{-1}. Given the 0.8 mm d^{-1} accuracy on the ASTER retrievals [2, 3], that of the Landsat ones was about 0.9 mm d^{-1}. Thus, the latter was close to the accuracy usually targeted [6, 23], in spite of differences between Landsat and ASTER retrievals for S-SEBI inputs.

We finally addressed the obtaining of close estimates of daily ET from both imageries in spite of differences between retrievals of S-SEBI inputs. A typical example is illustrated with Fig. 1 for 15 Sep 2007. For S-SEBI inputs, we noted differences between T_S and α retrievals from the two imageries as exemplified for T_S in Fig. 1a. However, both instruments captured similar spatial patterns for α and T_S, as illustrated in the T_S-α scatterplots (Fig. 1c and 1d). Thus, the spatial differencing in temperature within each albedo class tended to minimize differences on inputs and therefore to provide similar estimates of daily ET (Fig. 1b).

VI. CONCLUDING REMARKS

Three main items have to be addressed as concluding remarks. First, we observed non-negligible differences between ASTER and Landsat retrievals of albedo and radiometric temperature, whereas these retrievals were derived from methods that are widely used to process ASTER and Landsat imageries. Second, we obtained similar Landsat and ASTER retrievals of daily ET, in spite of differences between retrievals of temperature and albedo from the two sensors. This was ascribed to the S-SEBI spatial differencing in temperature that permitted to offset systematic differences. Third, daily ET could be retrieved from the two imageries with an accuracy close to that regularly targeted for further applications, even for row crops such as vineyards. Thus, it seems possible to use historical Landsat time series to assess seasonal, inter-annual and long-term trends in daily ET within vineyard landscapes.

REFERENCES

[1] D. P. Roy, M. A. Wulder, T. R. Loveland, C. E. Woodcock, R. G. Allen, M. C. Anderson, *et al.*, "Landsat-8: Science and product vision for terrestrial global change research," *Remote Sensing of Environment,* vol. 145, pp. 154-172, April 2014.

[2] M. Galleguillos, F. Jacob, L. Prévot, A. French, and P. Lagacherie, "Comparison of two temperature differencing methods to estimate daily evapotranspiration over a Mediterranean vineyard watershed from ASTER data," *Remote Sensing of Environment,* vol. 115, pp. 1326-1340, June 2011.

[3] M. Galleguillos, F. Jacob, L. Prévot, P. Lagacherie, and L. Shunlin, "Mapping Daily Evapotranspiration Over a Mediterranean Vineyard Watershed," *Geoscience and Remote Sensing Letters, IEEE,* vol. 8, pp. 168-172, January 2011.

[4] K. A. Semmens, M. C. Anderson, W. P. Kustas, F. Gao, J. G. Alfieri, L. McKee, *et al.*, "Monitoring daily evapotranspiration over two California vineyards using Landsat 8 in a multi-sensor data fusion approach," *Remote Sensing of Environment,* vol. 185, pp. 155-170, 11// 2016.

[5] B. Gallego-Elvira, A. Olioso, M. Mira, S. R. Castillo, G. Boulet, O. Marloie, *et al.*, "EVASPA (EVapotranspiration Assessment from SPAce)

Tool: An overview," *Procedia Environmental Sciences,* vol. 19, pp. 303-310, June 2013.

[6] B. Seguin, F. Becker, T. Phulpin, X. F. Gu, G. Guyot, Y. Kerr*, et al.*, "IRSUTE: A Minisatellite Project for Land Surface Heat Flux Estimation from Field to Regional Scale," *Remote Sensing of Environment,* vol. 68, pp. 357-369, June 1999.

[7] A. Ershadi, M. F. McCabe, J. P. Evans, and J. P. Walker, "Effects of spatial aggregation on the multi-scale estimation of evapotranspiration," *Remote Sensing of Environment,* vol. 131, pp. 51-62, April 2013.

[8] Y. Ryu, D. D. Baldocchi, T. A. Black, M. Detto, B. E. Law, R. Leuning*, et al.*, "On the temporal upscaling of evapotranspiration from instantaneous remote sensing measurements to 8-day mean daily-sums," *Agricultural and Forest Meteorology,* vol. 152, pp. 212-222, January 2012.

[9] A. French, F. Jacob, M. Anderson, W. Kustas, W. Timmermans, A. Gieske*, et al.*, "Surface energy fluxes with the Advanced Spaceborne Thermal Emission and Reflection radiometer (ASTER) at the Iowa 2002 SMACEX site (USA)," *Remote Sensing of Environment,* vol. 99, pp. 55-65, November 2005.

[10] M. Mira, T. J. Schmugge, E. Valor, V. Caselles, and C. Coll, "Analysis of ASTER Emissivity Product Over an Arid Area in Southern New Mexico, USA," *Geoscience and Remote Sensing, IEEE Transactions on,* vol. 49, pp. 1316-1324, April 2011.

[11] F. Jacob, A. Olioso, X. F. Gu, Z. Su, and B. Seguin, "Mapping surface fluxes using airborne visible, near infrared, thermal infrared remote sensing data and a spatialized surface energy balande model," *Agronomie-Sciences des Productions Vegetales et de l'Environnement,* vol. 22, pp. 669-680, September 2002.

[12] N. Bhattarai, S. B. Shaw, L. J. Quackenbush, J. Im, and R. Niraula, "Evaluating five remote sensing based single-source surface energy balance models for estimating daily evapotranspiration in a humid subtropical climate," *International Journal of Applied Earth Observation and Geoinformation,* vol. 49, pp. 75-86, July 2016.

[13] W. Ma, M. Hafeez, U. Rabbani, H. Ishikawa, and Y. Ma, "Retrieved actual ET using SEBS model from Landsat-5 TM data for irrigation area of Australia," *Atmospheric Environment,* vol. 59, pp. 408-414, November 2012.

[14] G. J. Roerink, Z. Su, and M. Menenti, "S-SEBI: A simple remote sensing algorithm to estimate the surface energy balance," *Physics and Chemistry of the Earth, Part B: Hydrology, Oceans and Atmosphere,* vol. 25, pp. 147-157, January 2000.

[15] N. Guix-Hébrard, M. Voltz, W. Trambouze, F. Garnier, J. P. Gaudillère, and P. Lagacherie, "Influence of watertable depths on the variation of grapevine water status at the landscape scale," *European Journal of Agronomy,* vol. 27, pp. 187-196, October 2007.

[16] M. Abrams, "The Advanced Spaceborne Thermal Emission and Reflection Radiometer (ASTER): Data products for the high spatial resolution imager on NASA's Terra platform," *International Journal of Remote Sensing,* vol. 21, pp. 847-859, January 2000.

[17] K. Thome, F. Palluconi, T. Takashima, and K. Masuda, "Atmospheric correction of ASTER," *Geoscience and Remote Sensing, IEEE Transactions on,* vol. 36, pp. 1199-1211, July 1998.

[18] A. Gillespie, S. Rokugawa, T. Matsunaga, J. S. Cothern, S. Hook, and A. B. Kahle, "A temperature and emissivity separation algorithm for Advanced Spaceborne Thermal Emission and Reflection Radiometer (ASTER) images," *Geoscience and Remote Sensing, IEEE Transactions on,* vol. 36, pp. 1113-1126, July 1998.

[19] E. F. Vermote, D. Tanre, J. L. Deuze, M. Herman, and J. J. Morcette, "Second Simulation of the Satellite Signal in the Solar Spectrum, 6S: an overview," *Geoscience and Remote Sensing, IEEE Transactions on,* vol. 35, pp. 675-686, May 1997.

[20] J. A. Barsi, J. R. Schott, F. D. Palluconi, and S. J. Hook, "Validation of a web-based atmospheric correction tool for single thermal band instruments," in *Proc. SPIE 5882, Earth Observing Systems X, 58820E (September 07, 2005)*, 2005.

[21] E. Kalnay, M. Kanamitsu, R. Kistler, W. Collins, D. Deaven, L. Gandin*, et al.*, "The NCEP/NCAR 40-Year Reanalysis Project," *Bulletin of the American Meteorological Society,* vol. 77, pp. 437-471, March 1996.

[22] B. N. Holben, D. Tanré, A. Smirnov, T. F. Eck, I. Slutsker, N. Abuhassan*, et al.*, "An emerging ground-based aerosol climatology: Aerosol optical depth from AERONET," *Journal of Geophysical Research: Atmospheres,* vol. 106, pp. 12067-12097, June 2001.

[23] J. Kalma, T. McVicar, and M. McCabe, "Estimating Land Surface Evaporation: A Review of Methods Using Remotely Sensed Surface Temperature Data," *Surveys in Geophysics,* vol. 29, pp. 421-469, October 2008.

[24] M. Weiss, F. Baret, M. Leroy, A. Bégué, O. Hautecoeur, and R. Santer, "Hemispherical reflectance and albedo estimates from the accumulation of across-track sun-synchronous satellite data," *Journal of Geophysical Research: Atmospheres,* vol. 104, pp. 22221-22232, September 1999.

[25] S. Liang, "Narrowband to broadband conversions of land surface albedo I: Algorithms," *Remote Sensing of Environment,* vol. 76, pp. 213-238, May 2001.

[26] W. Brutsaert, "On a derivable formula for long-wave radiation from clear skies," *Water Resources Research,* vol. 11, pp. 742-744, October 1975.

[27] K. Ogawa, T. Schmugge, F. Jacob, and A. French, "Estimation of land surface window (8–12 μm) emissivity from multi-spectral thermal infrared remote sensing — A case study in a part of Sahara Desert," *Geophysical Research Letters,* vol. 30, p. 1067, January 2003.

[28] C. Cammalleri, M. C. Anderson, G. Ciraolo, G. D'Urso, W. P. Kustas, G. La Loggia*, et al.*, "The impact of in-canopy wind profile formulations on heat flux estimation in an open orchard using the remote sensing-based two-source model," *Hydrol. Earth Syst. Sci.,* vol. 14, pp. 2643-2659, 2010.

[29] B. J. Choudhury, N. U. Ahmed, S. B. Idso, R. J. Reginato, and C. S. T. Daughtry, "Relations between evaporation coefficients and vegetation indices studied by model simulations," *Remote Sensing of Environment,* vol. 50, pp. 1-17, 1994/10/01 1994.

[30] J. C. Jimenez-Munoz, J. Cristobal, J. A. Sobrino, G. Soria, M. Ninyerola, and X. Pons, "Revision of the Single-Channel Algorithm for Land Surface Temperature Retrieval From Landsat Thermal-Infrared Data," *IEEE Transactions on Geoscience and Remote Sensing,* vol. 47, pp. 339-349, 2009.

[31] A. Olioso, "Estimating the difference between brightness and surface temperatures for a vegetal canopy," *Agricultural and Forest Meteorology,* vol. 72, pp. 237-242, January 1995.

[32] K. Ogawa, T. Schmugge, F. Jacob, and A. French, "Estimation of broadband land surface emissivity from multi-spectral thermal infrared remote sensing," *Agronomie,* vol. 22, pp. 695-696, September 2002.

[33] M. Gómez, A. Olioso, J. A. Sobrino, and F. Jacob, "Retrieval of evapotranspiration over the Alpilles/ReSeDA experimental site using airborne POLDER sensor and a thermal camera," *Remote Sensing of Environment,* vol. 96, pp. 399-408, June 2005.

[34] M. Mira, A. Olioso, B. Gallego-Elvira, D. Courault, S. Garrigues, O. Marloie*, et al.*, "Uncertainty assessment of surface net radiation derived from Landsat images," *Remote Sensing of Environment,* vol. 175, pp. 251-270, March 2016.

[35] A. Bsaibes, D. Courault, F. Baret, M. Weiss, A. Olioso, F. Jacob*, et al.*, "Albedo and LAI estimates from FORMOSAT-2 data for crop monitoring," *Remote sensing of environment,* vol. 113, pp. 716-729, April 2009.

[36] F. Jacob and A. Olioso, "Derivation of diurnal courses of albedo and reflected solar irradiance from airborne POLDER data acquired near solar noon," *Journal of Geophysical Research: Atmospheres (1984–2012),* vol. 110, 2005.

[37] M. Mira, M. Weiss, F. Baret, D. Courault, O. Hagolle, B. Gallego-Elvira*, et al.*, "The MODIS (collection V006) BRDF/albedo product MCD43D: Temporal course evaluated over agricultural landscape," *Remote Sensing of Environment,* vol. 170, pp. 216-228, December 2015.

[38] F. Jacob, T. Schmugge, A. Olioso, A. French, D. Courault, K. Ogawa*, et al.*, "Modeling and inversion in thermal infrared remote sensing over vegetated land surfaces," in *Advances in Land Remote Sensing*, ed: Springer, 2008, pp. 245-291.

[39] C. Coll, J. M. Galve, J. M. Sanchez, and V. Caselles, "Validation of Landsat-7/ETM+ Thermal-Band Calibration and Atmospheric Correction With Ground-Based Measurements," *Geoscience and Remote Sensing, IEEE Transactions on,* vol. 48, pp. 547-555, January 2010.

[40] Z.-L. Li, B.-H. Tang, H. Wu, H. Ren, G. Yan, Z. Wan*, et al.*, "Satellite-derived land surface temperature: Current status and perspectives," *Remote Sensing of Environment,* vol. 131, pp. 14-37, April 2013.

[41] C. Mattar, B. Franch, J. A. Sobrino, C. Corbari, J. C. Jiménez-Muñoz, L. Olivera-Guerra*, et al.*, "Impacts of the broadband albedo on actual evapotranspiration estimated by S-SEBI model over an agricultural area," *Remote Sensing of Environment,* vol. 147, pp. 23-42, May 2014.